NRC Research Press

ARTICLE

Glacier velocities and dynamic discharge from the ice masses of Baffin Island and Bylot Island, Nunavut, Canada

Wesley Van Wychen, Luke Copland, David O. Burgess, Laurence Gray, and Nicole Schaffer

Abstract: Speckle tracking of ALOS PALSAR fine beam data from 2007–2011 are used to determine the surface motion of major ice masses on Baffin Island and Bylot Island in the southern Canadian Arctic Archipelago. Glacier velocities are low overall, with peaks of ~100 m a^{-1} and means of ~20–60 m a^{-1} common along the main trunk of many outlet glaciers. Peak velocities on Penny and Bylot Island ice caps tend to occur near the mid-sections of their primary outlet glaciers, while the fastest velocities on all other glaciers usually occur near their termini due to relatively large accumulation areas draining through narrow outlets. Estimates of ice thickness at the fronts of tidewater-terminating glaciers are combined with the velocity measurements to determine a regional dynamic discharge rate of between ~17 Mt a^{-1} and ~108 Mt a^{-1}, with a mid-point estimate of ~55 Mt a^{-1}, revising downward previous approximations. These velocities can be used as inputs for glacier flow models, and provide a baseline dataset against which future changes in ice dynamics can be detected.

Résumé : Le suivi speckle des données de faisceau fin ALOS PALSAR, prélevées entre 2007 et 2011, est utilisé pour déterminer le mouvement de surface des grandes masses de glace sur les îles de Baffin et de Bylot dans le sud de l'archipel arctique canadien. Les vitesses des glaciers sont généralement faibles avec des pointes d'environ 100 m a^{-1} et des moyennes de 20 à 60 m a^{-1} fréquentes le long du tronc principal de nombreux glaciers émissaires. Les vitesses de pointe des champs de glace de Penny et de Bylot tendent à être près des sections médianes de leurs glaciers émissaires primaires, alors que les vitesses les plus rapides sur tous les autres glaciers sont enregistrées près du front en raison des aires d'accumulation relativement grandes qui s'écoulent à travers d'étroites décharges. Des estimations de l'épaisseur de la glace aux fronts de glaciers de marée sont combinées aux mesures de vitesse afin de déterminer un taux régional de décharge dynamique entre ~17 Mt a^{-1} et ~108 Mt a^{-1}, avec une estimation du taux médian de ~55 a^{-1}, ce qui révise les estimations antérieures à la baisse. Ces vitesses peuvent être utilisées comme données d'entrée pour les modèles d'écoulement glaciaire et ainsi fournir un ensemble de données de référence pour détecter les futurs changements dans la dynamique glaciaire. [Traduit par la Rédaction]

Introduction

The southern Canadian Arctic Archipelago (CAA), consisting of Baffin Island and Bylot Island (Fig. 1), contain ~40 000 km^2 of glacier ice (Gardner et al. 2012). Recent studies indicate that these ice masses are undergoing substantial change. Passive microwave records reveal that the average melt season on Barnes Ice Cap lengthened by ~33% between 1979–1987 and 2002–2010, and nearly doubled on Penny Ice Cap between 1979 and 2010 (Dupont et al. 2012; Zdanowicz et al. 2012). Firn temperatures at 10 m depth near the summit of Penny Ice Cap have warmed by ~10 °C between the mid-1990s and 2011, and recent surface melt rates are comparable to those experienced over 3000 years ago (Zdanowicz et al. 2012). Geodetic methods indicate surface lowering of up to ~1 m a^{-1} on all ice masses on Baffin Island and Bylot Island between 1963 and 2006, with greatest surface lowering concentrated on ice mass margins and low-lying outlet glaciers (Gardner et al. 2012). From 2003 to 2011 the glaciers of the southern CAA lost ice at a rate of 23.8 ± 6.12 Gt a^{-1} and contributed 0.07 ± 0.02 mm a^{-1} to global sea level rise over this period (accounting for 16% of the total contribution from ice masses outside of the ice sheets) (Gardner et al. 2012). There has been little change in regional precipitation and the main driver of accelerated ice loss has been an increase in summer air temperatures, with models projecting sustained mass loss within the region over the next century (Gardner et al. 2012; Lenaerts et al. 2013).

Despite the large area and volume of glacial ice contained within Baffin Island and Bylot Island, no previous regional survey of glacier and ice cap motion has been undertaken. Only a single estimate of dynamic discharge has been previously reported (~0.25 Gt a^{-1}, equivalent to 250 Mt a^{-1}) based on the average ice flux per terminus width derived from sparse velocity data from the northern CAA (Gardner et al. 2011). As a consequence, our knowledge of ice dynamics over a large portion of the Canadian Arctic is presently limited, and the current estimate of mass loss via dynamic discharge from Baffin Island and Bylot Island is poorly constrained. Here we use speckle tracking of ALOS PALSAR fine beam (~9 m) RADAR imagery acquired between 2007 and 2011 to determine surface displacements and produce the first comprehensive velocity map for the major ice masses of the southern CAA. At the terminus of tidewater glaciers, surface ice velocities and estimated ice thicknesses (bounded by measurements from analogous glaciers by NASA's operation IceBridge) are used to calculate mass loss via dynamic discharge. Here dynamic discharge is defined as mass loss via iceberg calving and subaque-

Received 7 May 2015. Accepted 19 July 2015.

Paper handled by Associate Editor Timothy Fisher.

W. Van Wychen. Department of Geography, University of Ottawa, Ottawa, ON K1N 6N5, Canada; Natural Resources Canada, Geological Survey of Canada, 601 Booth St., Ottawa, ON K1A 0E8, Canada.
L. Copland, L. Gray, and N. Schaffer. Department of Geography, University of Ottawa, Ottawa, ON K1N 6N5, Canada.
D.O. Burgess. Natural Resources Canada, Geological Survey of Canada, 601 Booth St., Ottawa, ON K1A 0E8, Canada.
Corresponding author: Wesley Van Wychen (e-mail: wesley.vanwychen@gmail.com).

Fig. 1. Location of the major ice masses of Baffin Island and Bylot Island (shown in green). Base Image: MODIS Terra, 2 July 2011. Dashed boxes indicate the extents of Figs. 2–4. Colour figures available online.

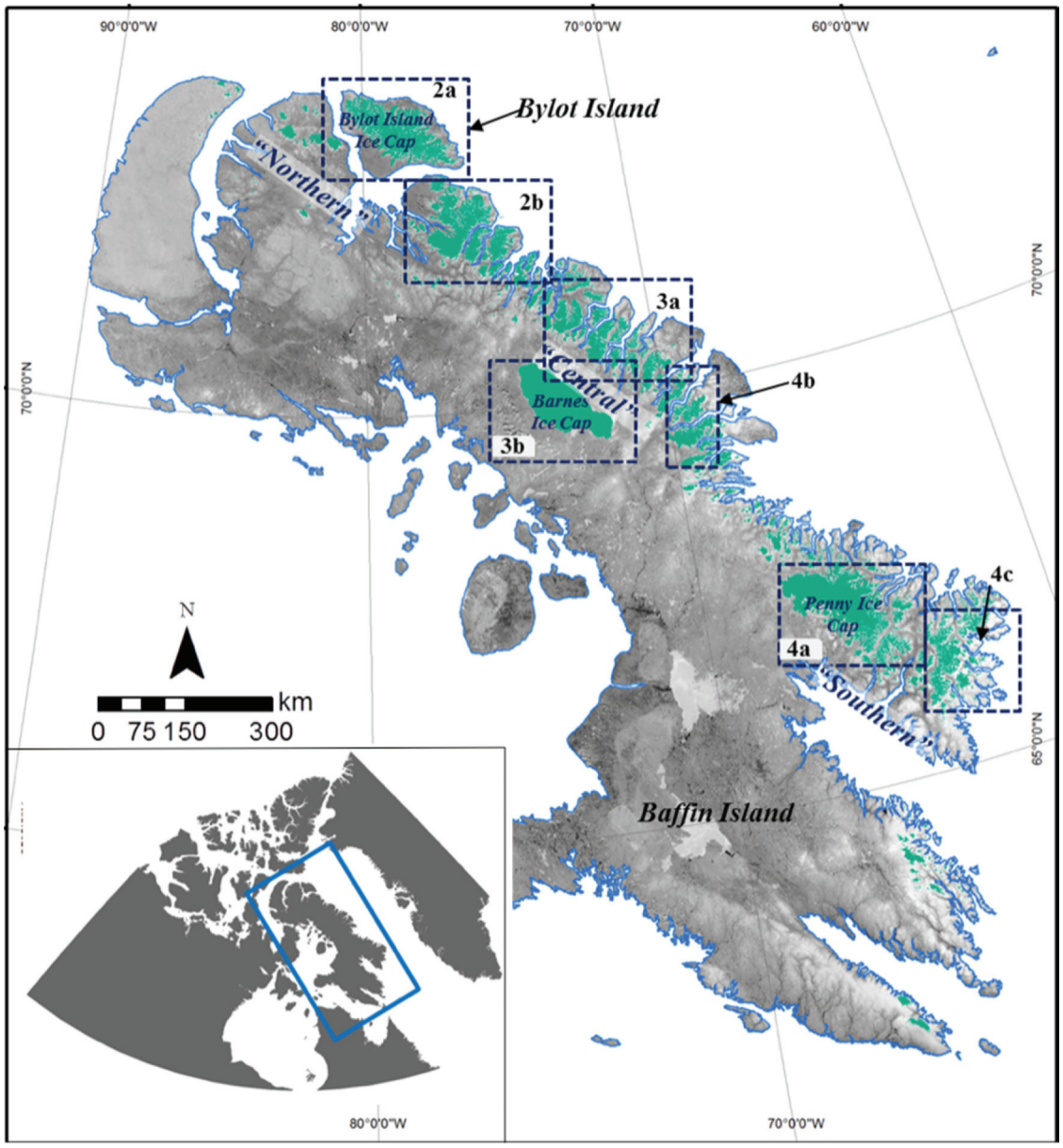

ous melt, following terminology consistent with other studies that utilize similar methods (e.g., Van Wychen et al. 2014).

Study site

The principal ice masses of the southern CAA are Bylot Island Ice Cap (4783 km² in 2000), Penny Ice Cap (6478 km² in 2000), Barnes Ice Cap (5874 km² in 2000), and the coastal glaciers (21 835 km² in 2000) that fringe Baffin Bay (Fig. 1). The Bylot Island Ice Cap occupies ~43% of Bylot Island and is dissected by the Byam Martin Mountains that extend the entire 150 km length of Bylot Island in a northwest–southeast direction (Dowdeswell et al. 2007). The distribution of glaciers reflects the island's topography, and consists of large outlet glaciers extending from the high elevation ice cap interior to the margins, separate remnant ice masses that have become detached from the ice cap proper, and isolated ice patches in low-lying areas (Dowdeswell et al. 2007). There are two unnamed glaciers that terminate into the ocean located in the northeastern portion of the ice cap, and 10 glaciers have been inferred as probable surge-type based on the identification of features that suggest previous surge activity (e.g., looped and deformed moraines, widespread crevassing, pronounced ice ramps, stagnant ice, potholes, and over-steepened glacier termini) (Dowdeswell et al. 2007).

Penny Ice Cap is the southernmost large ice mass of the CAA and is a partial remnant of the Laurentide Ice Sheet (Zdanowicz et al. 2012). Major glaciers radiate outward from the ice cap interior through constrained valleys toward the north, east, and south. In the northwest the ice cap terminates in a broad, lobe-like region. The surface velocity structure of seven outlet glaciers has previously been determined utilizing optical feature tracking, with the finding that ice motion had generally slowed between the mid-1980s and mid-2000s due to a long-term negative mass balance (Heid and Kääb 2012). There are two tidewater-terminating glaciers on Penny Ice Cap: Coronation Glacier located in the southeast, and an unnamed glacier located in the north-central region.

Barnes Ice Cap, also a remnant of the Laurentide Ice Sheet, is a dome-shaped ice mass situated in the interior of Baffin Island on a broad plateau (Dupont et al. 2012; Sharp et al. 2014). Maximum ice elevation rises to ~1100 m a.s.l. and the margins terminate at ~500 m a.s.l. (Dupont et al. 2012). The majority of the ice cap terminates on land in a broad lobe-like structure, although small regions terminate in lakes located in the north and south. "Surge scars" have been used to infer past surging in the southwest of the ice cap, and measurements of basal ice temperature indicated ice at pressure melting point, providing a mechanism that would facilitate sliding (Holdsworth 1977).

There are a large number of smaller ice caps and glaciers that fringe the northern and eastern coastline of Baffin Island. Typically, these ice masses are characterized by a few outlet glaciers (some of which are tidewater terminating) that drain small ice caps through confined valleys. The larger coastal outlet glaciers have widths of ~1–3 km and in some cases extend ~30 km into ice cap interiors. Our velocity mapping covers ~93% of the glaciated area of Baffin Island and Bylot Island. It notably excludes the Terra Nivea and Grinnell ice caps and the smaller coastal ice masses that fringe the far southern parts of Baffin Island, due to a lack of SAR imagery suitable for deriving glacier motion there.

Table 1. Summary of ALOS PALSAR imagery used in this study.

Image date 1 (dd-mm-yyyy)	Image date 2 (dd-mm-yyyy)	Image segments	Region
08-01-2011	23-02-2011	2	Barnes Ice Cap (west)
25-03-2007	10-05-2007	6	Barnes Ice Cap (east), coastal glaciers
19-12-2010	03-02-2011	2	Penny Ice Cap (west)
01-03-2010	04-16-2010	3	Penny Ice Cap (central)
31-12-2010	15-02-2011	2	Penny Ice Cap (east)
12-01-2011	27-02-2011	2	Southeast Baffin Island
24-01-2011	11-03-2011	2	Southeast Baffin Island
08-01-2011	23-02-2011	4	Bylot Island Ice Cap (east)
30-01-2011	17-03-2011	3	Bylot Island Ice Cap (west)
06-01-2011	21-02-2011	1	Northwest Baffin Island
28-01-2011	15-03-2011	1	Northwest Baffin Island
29-12-2010	13-02-2011	2	Central Baffin Island coastline
10-01-2011	25-02-2011	3	Central Baffin Island coastline
22-10-2011	07-12-2011	3	Central Baffin Island coastline

Note: All imagery was 9 m resolution, and all beam modes were fine beam single polarization, except for a single pair (22-10-2011 to 07-12-2011), which was fine beam double polarization.

Methods

Determination of surface motion

ALOS PALSAR data were obtained in Level 0 CEOS format from the Alaska Satellite Facility's Vertex Data Portal (https://vertex.daac.asf.alaska.edu/) from 2007–2011 (Table 1). ALOS PALSAR L-band data have proven effective for determining surface motion for temperate ice masses (e.g., Burgess et al. 2013), and imagery was acquired during winter months when changes to the glacier surface that affect coherence are minimized (e.g., snowfall, rainfall, melt). The Level 0 data were processed to Single Look Complex format using the GAMMA Modular SAR Processor, and surface motion was derived using a custom-written MATLAB algorithm that estimates azimuth and slant range displacements between image pairs, and references these displacements to zero motion areas. If the conditions for interferometry are satisfied (Rosen et al. 2000) and the near surface conditions have not changed significantly between the times of data acquisition (a multiple of the 46-day ALOS repeat cycle), then the speckle pattern in the two images will be correlated (Gray et al. 2001). This approach is advantageous because if distinct image features (e.g., crevasses) exist in the image pair then the "speckle tracking" algorithm will degrade to less accurate feature tracking, even if coherence between the two images is poor. This can then be described more generally as "offset" tracking (Strozzi et al. 2002). However, we find that L-band imagery (e.g., ALOS) maintains coherence for longer time periods than C-band imagery (e.g., Radarsat) and that the majority of our results were obtained with speckle tracking, so we use this term for our description of the processing methodology.

To preserve bandwidth, and, therefore, image resolution, the complex SLC data were up-sampled by a factor of two in both range and azimuth, in the latter case taking account of the Doppler centroid frequency. After estimating a coarse image-to-image registration, image chips were selected from the master (earlier) image and a two-dimensional search was performed to identify the corresponding region in the second image. The resulting normalized two-dimensional cross-correlation function is up-sampled and the peak is used to give the best estimates of the range and azimuth shifts. This approach has previously been used to determine glacier displacement in the Canadian High Arctic (Short and Gray 2005; Van Wychen et al. 2012, 2014) and Yukon/Alaska (Waechter et al. 2015). Image chip size is variable, but in this case it was ~400 m in both azimuth and ground range direction, with overlap of 50% between adjacent chips. Because the orbits are not repeated perfectly there can be a stereo component in the slant range direction due to the perpendicular baseline (Rosen et al. 2000), which leads to a topography dependent range displacement not associated with surface motion. The 1:250 000 Canadian Digital Elevation Dataset (CDED) was used to remove this topographic component of slant range displacement and even with a relatively large perpendicular baseline the accuracy of the CDED data are adequate to minimize any possible error. To remove systematic biases due to inaccuracies in satellite baseline estimates or squint effects between image acquisitions, displacements were calibrated using areas of zero motion (bedrock outcrops) to determine the local bias, which is then removed from the rest of the dataset. A further erroneous azimuth shift problem can arise, particularly with L-band SAR data, due to ionospheric disturbances (Gray et al. 2000). In this case, care is taken to identify adjacent no-motion areas (e.g., bedrock on either side of an outlet glacier) to try to minimize any bias error in the azimuth shift not due to ice movement and remove this bias from the areas locally affected by streaking.

The MATLAB speckle tracking code utilized outputs a text file of geocoded point vectors of the strongest correlations between image chips in the master and slave images that were then imported into ArcGIS for verification and filtering of erroneous matches. Mismatch errors occur when the speckle tracking algorithm finds a stronger correlation with an incorrect image chip other than the "true" match. To identify and remove these errors from the velocity dataset, manual inspection and verification of the results was undertaken within ArcGIS 10.1 on all velocity results. Once mismatches were removed from the dataset the velocities were converted to a continuous raster surface (100 × 100 m pixels), using an inverse distance-weighting interpolation, which does not create pixel values beyond measured displacements. Rasters of surface ice velocity are mosaicked (using a minimum value in areas of overlap) into a single velocity dataset for each individual ice mass, and final raster datasets were clipped to the extent of the GLIMS Randolph Glacier Inventory (version 3.2, representing glacier extents in years ~1999–2001; available online: http://www.glims.org/RGI/). The use of an IDW interpolation method combined with the minimum values in areas of overlap is consistent with previous methods of creating continuous rasters of glacier surface velocities in the Canadian High Arctic (Van Wychen et al. 2012, 2014). This means that the surface velocities presented here are conservative and may slightly underestimate rates of ice motion and dynamic discharge.

Error analysis

To provide an indication of the reliability of the speckle tracking results, velocities were extracted over known stationary regions (bedrock outcrops and ice divides). Mean displacement over 8 536 449 unique bedrock points yielded a mean value of 5.4 m a^{-1} and standard deviation of 4.9 m a^{-1}. Mean displacement over 32 518 unique ice divide locations (extracted from RGI v3.2) yielded a mean value of 5.1 m a^{-1} and standard deviation of 2.9 m a^{-1}. These error estimates are within ranges previously reported when using the same speckle tracking algorithm on Radarsat-2 data in the Canadian High Arctic (Van Wychen et al. 2012, 2014).

In situ surveys of the motion of mass balance stakes on Penny Ice Cap between spring 2011 and 2012 provide validation for the remote sensing results and an assessment of how well velocities derived from winter ALOS data over a 46-day period represent annual motion. The stake positions were measured with a Trimble R7 dGPS unit, with the antenna inserted into the top of each mass balance stake for a period of 20–30 min during each visit. The dGPS data were post-processed with Natural Resources Canada's online Precise Point Positioning service (http://webapp.geod.nrcan.gc.ca/geod/tools-outils/ppp.php), and results are considered accurate within ±0.15 m horizontally. The mean absolute difference between 23 in situ measurements of surface ice displacement and those determined by speckle tracking was 7.9 m a^{-1} (Table 2). Sixty percent (14 of 23) of the displacements derived from speckle tracking were within the error margins determined over stationary locations and ~90% (21 of 23) of the displacements derived from speckle tracking were within 15 m a^{-1}. The two locations with the greatest discrepancy (~21.5 m a^{-1}) between the two methods occurred on the lower sections of Coronation Glacier, where melt likely induces summer acceleration that is not captured in the winter-only speckle tracking measurements.

Each method of determining reliability of surface velocities has drawbacks: bedrock outcrops provide estimates of motion over non-moving regions that may not be representative of areas of motion, ice divides are poorly defined within the Canadian Arctic and as such may not provide exact locations of zero motion, and comparisons with in situ dGPS measurements and speckle tracking results are inexact due to the difference between monitoring periods (~1 year versus 46 days). Thus, to provide an estimate of confidence in our velocity results, we use the root sum of squares from all the separate sources of error (bedrock outcrops, ice divides, and displacement stakes). This analysis yields ~±8.5 m a^{-1} as the uncertainty in the velocity dataset.

Determination of dynamic discharge

To quantify dynamic discharge from the study region, a visual assessment of Landsat 7/8 imagery and review of previous studies (e.g., Randolph Glacier Inventory; Gardner et al. 2011) was undertaken to identify which glaciers are tidewater terminating. This identified a total of 46 glaciers (denoted on Figs. 2–4) that terminate in the ocean. Ice thickness information is needed to compute ice flux, but there is a sparse availability of ice thickness data on Baffin Island and Bylot Island. We, therefore, adopted a scenario-based approach, where ice depths for flux gates at glacier termini are modeled based on the available measurements of analogous glaciers within the study region.

We use two different scenarios to distinguish between the morphology of large glaciers ("outlet glaciers"), which descend from ice mass interiors to the coastal margins, and the morphology of smaller glaciers ("valley glaciers") that drain from relatively small accumulation areas to the ocean. For both scenarios, ice flux gates at the glacier termini are based on low, high, and midpoint measurements of ice depths on analogous glaciers within the study region. For the outlet glaciers scenario, values were chosen based on airborne ice thickness measurements determined by NASA's Operation Icebridge (acquired 5 and 12 May 2011; ftp://data.cresis.ku.edu/data/rds/) along the lower (~15–20 km) terminus region of four large glaciers that descend from the interior of Bylot Island to the margins. This dataset provides a total of 4556 unique measurements with a mean ice thickness of ~276 m (minimum of 29.8 m and maximum of 413.9 m). Measured ice thicknesses less than 100 m are restricted to small isolated pockets along two glaciers, while measured ice thicknesses greater than 300 m tend to occur in higher elevation regions and are less likely to reflect the terminus glacier morphology. As such, we use the average of these values to establish a low thickness estimate of 100 m, a high estimate of 300 m, and a midpoint estimate of 200 m.

Table 2. Comparison of displacements derived from in situ (dGPS) and speckle tracking on a transect across Penny Ice Cap (location of dGPS stations are denoted in Fig. 4*a*).

			Displacement (m a^{-1})		
Lat. (°N)	Long. (°W)	dGPS ID	dGPS (2011–2012)	Speckle tracking (2011)	Difference
67.28	−65.85	P000	1.6	1.8	0.3
67.25	−65.88	P101	1.7	1.1	−0.6
67.23	−65.91	P102	9.0	9.2	0.3
67.22	−65.96	P103	16.1	18.9	2.8
67.21	−65.97	P104	20.8	17.9	−3.0
67.20	−66.02	P105	34.8	47.9	13.1
67.16	−66.13	P107	9.4	9.1	−0.4
67.15	−66.16	P108	80.9	91.6	10.8
67.13	−66.19	P109	102.5	103.4	0.9
67.09	−66.23	P111	82.7	82.8	0.0
67.07	−66.26	P112	80.1	84.0	3.9
66.86	−66.26	P120	38.4	34.4	−4.0
67.29	−65.85	P201	2.3	6.9	4.6
67.34	−65.85	P202	1.6	1.4	−0.1
67.39	−65.83	P203	1.6	8.0	6.4
67.42	−65.75	P204	1.3	7.7	6.4
67.43	−65.67	P205	2.8	6.7	3.9
67.03	−65.26	CG01	91.4	105.2	13.8
67.06	−65.16	CG02	58.3	37.0	−21.3
67.13	−64.99	CG03	43.9	21.9	−22.0
67.14	−65.02	CG04	27.2	23.3	3.9
67.19	−64.87	CG05	44.1	30.9	−13.2
67.19	−64.83	CG06	47.8	34.8	−13.1
Mean difference (absolute)					7.9

For the valley glaciers scenario, a low thickness estimate of 75 m was used based on 50 MHz ground penetrating radar measurements at the terminus of Fountain Glacier, Bylot Island, in 2007–2008 (Wainstein et al. 2014), while an upper limit of 150 m is based on the mean of 105 point ice thickness measurements determined by NASA's Operation Icebridge on 12 April 2013 on four valley glaciers (locations: 66.7°N, −65.2°W; 66.6°N, −65.1°W; 66.6°N, −65.1°W; 66.5°N, −65.3°W) located in southern Penny Ice Cap. A midpoint estimate of 112.5 m is then taken as the average of these values.

To approximate the shape of the glacier cross-section at each flux gate, we use the methodology of Van Wychen et al. (2014), who assumed a U-shaped morphology based on measurements of glaciers in the Canadian High Arctic (Gogineni 2012) and modeling of valley form after periods of erosion (Harbor 1992). The U-shaped morphology was modeled based upon the following:

$$T = \left[(10 - C)/D_1^2\right] \times \left(D_2^2\right) + C \quad (1)$$

where T is the assumed ice thickness using a parabolic interpolation based on the ice thickness scenarios at the glacier centerline (C_{min} = 75 m/100 m, C_{mid} = 112.5 m/200 m, C_{max} = 150 m/300 m; first presented ice depth value represents the valley glacier scenario and the second represents the outlet glacier scenario for C_{min}, C_{mid}, and

Fig. 2. Surface velocity structure of (*a*) Bylot Island Ice Cap and (*b*) and the coastal glaciers of northern Baffin Island. Standalone numbers denote glacier IDs presented in Table 3. White dashed lines and standalone letters indicate the location of extracted centerline velocities presented in Fig. 5. Base Image: MODIS Terra, 2 July 2011. Colour figures available online.

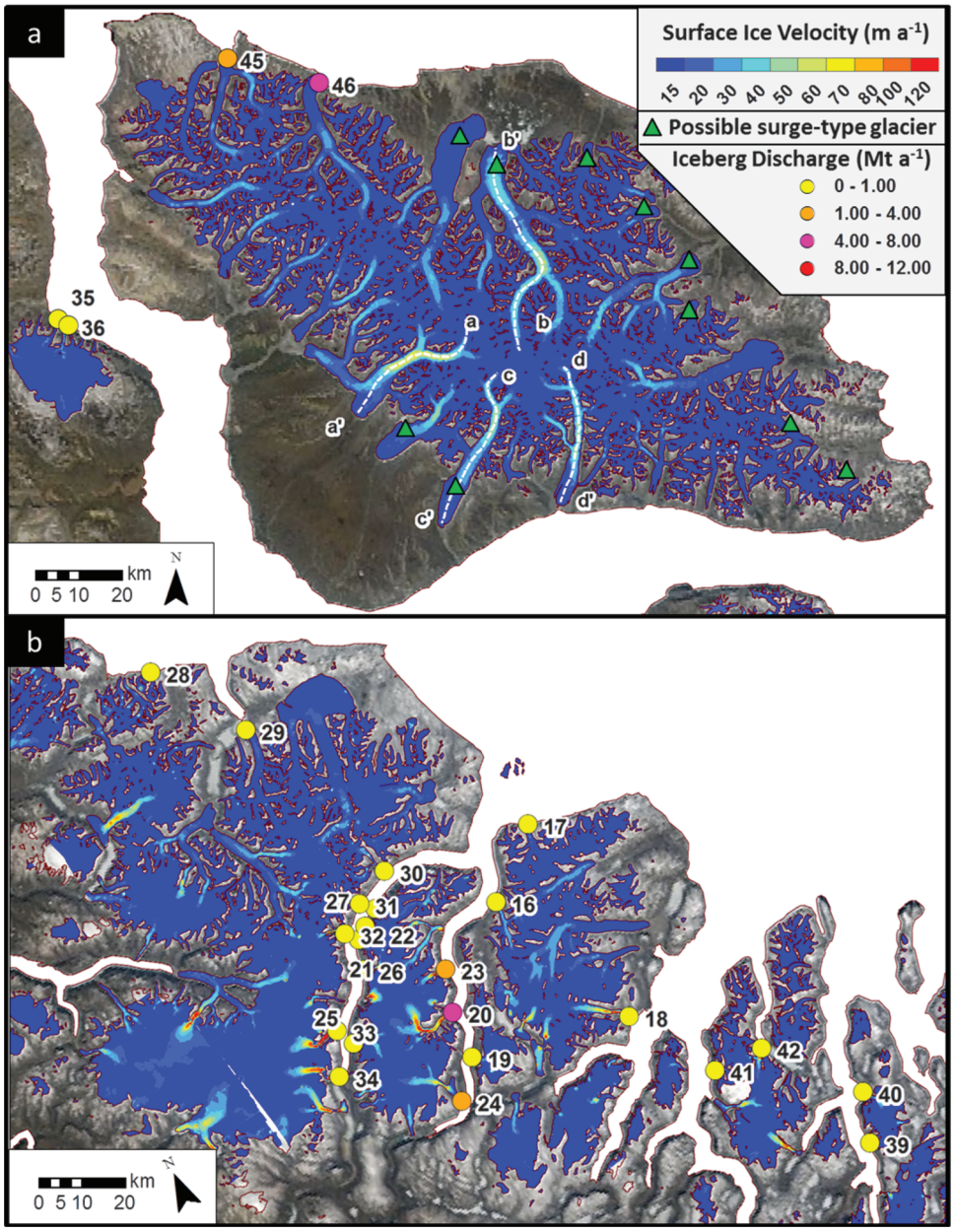

C_{max}), and a marginal 10 m ice thickness, D_1 is the distance from the glacier centreline to the margin, and D_2 is the distance from the centreline to the centre of the interpolated ice column. Ice column thicknesses are interpolated at 20 m intervals from the centreline to the glacier margins, and the surface motion of each ice column is extracted from the raster of surface velocity at each of these locations (20 m intervals are used to maintain consistency and comparability with interpolated flux gates created in the northern CAA (e.g., Van Wychen et al. 2014)). Low (Q_{min}), medium (Q_{mid}), and high (Q_{max}) discharge estimates for each column are then calculated using the following equations:

$$Q_{min} = [(V - V_{error}) \times 0.8] \times (T_{min}) \times (W) \quad (2)$$

$$Q_{mid} = (V) \times (T_{mid}) \times (W) \quad (3)$$

$$Q_{max} = (V + V_{error}) \times (T_{max}) \times (W) \quad (4)$$

where V is the extracted surface ice velocity measurement derived from speckle tracking, V_{error} is the error associated with the speckle tracking dataset (8.5 m a^{-1}; previously discussed above), and W is the ice column width (20 m). For the Q_{min} ice flux estimate we assume a depth-averaged velocity of 80% of the measured surface velocity to account for internal deformation (Paterson 1994), while for the Q_{mid} and Q_{max} estimates we assume that the motion at the glacier terminus is due to sliding alone and that the depth-averaged velocity is equal to the surface velocity.

Total Q_{min}, Q_{mid}, and Q_{max} estimates for each cross section are calculated from the sum of individual ice columns and are converted to units of Mt a^{-1} (1 Mt = 0.001 Gt). This method of calculat-

Fig. 3. Surface velocity structure of (*a*) the central coastal glaciers of Baffin Island and (*b*) Barnes Ice Cap. Standalone numbers denote glacier IDs presented in Table 3. White dashed lines and standalone letters indicate the location of extracted centerline velocities presented in Fig. 5. Base Image: MODIS Terra, 2 July 2011. Colour figures available online.

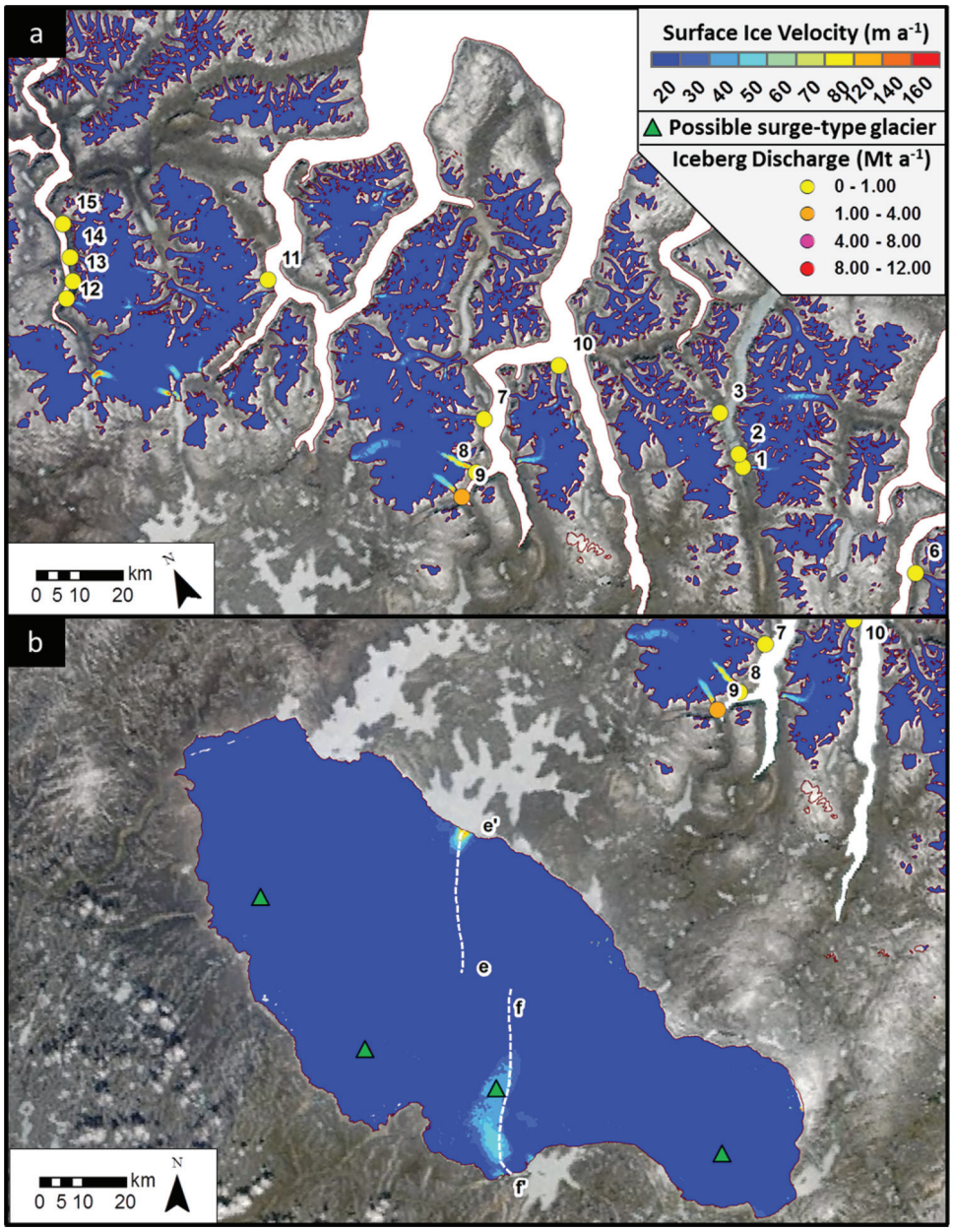

ing iceberg discharge is consistent with previous methods in the Canadian High Arctic (Burgess et al. 2005; Van Wychen et al. 2012, 2014). Other methods of estimating cross-sectional flux include using a box-shaped glacier geometry rather than a U-shaped glacier geometry (e.g., Williamson et al. 2008) or an ice-flux per unit of terminus width approach using estimated discharge rates from nearby areas and extrapolating them to other areas (e.g., Gardner et al. 2012). Our method is superior to these as it uses a more realistic glacier geometry (Harbor 1992) and because it uses measured glacier velocities rather than velocities extrapolated from other regions that may not represent the ice dynamics of the region of interest.

Results and discussion

Glacier velocity structure of Baffin Island and Bylot Island

Surface velocities of the ice masses of Baffin Island and Bylot Island are generally low (Figs. 2–4), with peak velocities of ~100 m a^{-1} and typical velocities of ~20–60 m a^{-1} along glacier centrelines. Surface motion of the interior of all ice caps is <20 m a^{-1}, suggestive of ice frozen to its bed and flowing by deformation only.

In the "northern" part of the study region (Fig. 2), velocities of ~40 m a^{-1} to 60 m a^{-1} are observed on four glaciers located in the south-central part of Bylot Island Ice Cap, and one in its north-central region (Figs. 2*a*, 5*a*–5*d*). Faster ice motion on these five land-terminating glaciers occurs near their middle sections (~750–1000 m a.s.l.), approximately coincident with the equilibrium line altitude (ELA ~800–900 m a.s.l. (Dowdeswell et al. 2007)). Ten glaciers on Bylot Island Ice Cap have previously been identified as possible surge type (indicated in Fig. 2) by Dowdeswell et al. (2007), and it is notable that three of the five faster flowing glaciers have been previously identified as surge type. The remaining seven glaciers previously identified as possi-

Fig. 4. Surface velocity structure of (*a*) Penny Ice Cap, (*b*) central coastal glaciers, and (*c*) southeastern coastal glaciers ("+" indicates locations of in situ dGPS observations and CG/P notations provide reference IDs referred to in Table 2). Standalone numbers denote glacier IDs presented in Table 3. White dashed lines and standalone letters indicate the location of extracted centerline velocities presented in Fig. 5. Base Image: MODIS Terra, 2 July 2011. Colour figures available online.

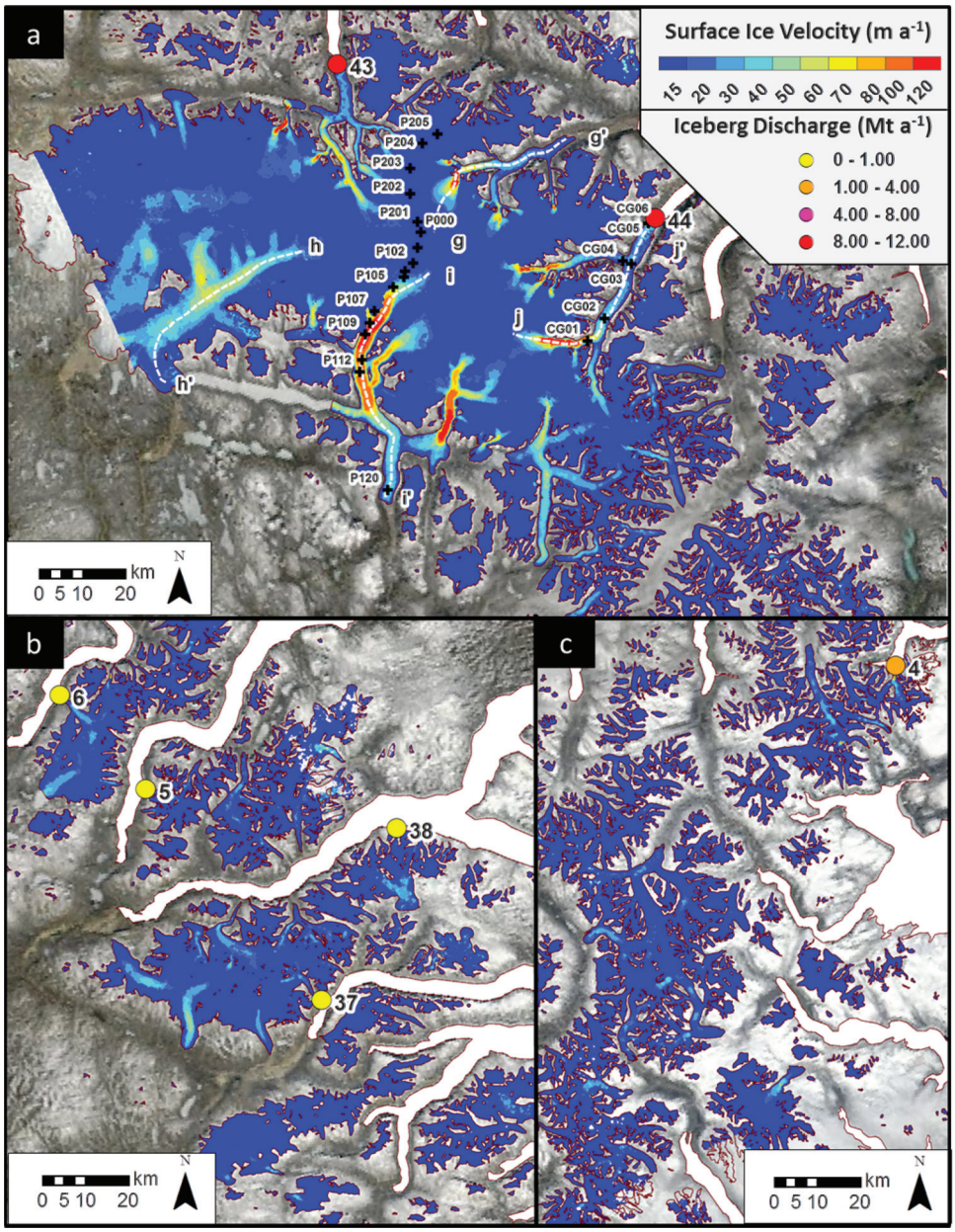

bly surge type have surface flow speeds of <20–30 m a^{-1}, which suggests that if they are surge type they are currently in their quiescent phase. For the coastal glaciers of northern Baffin Island (Fig. 2*b*), surface motion of 80–140 m a^{-1} occurs on several glaciers in locations where relatively large accumulation areas connect to narrow tributaries and outlet glaciers. These areas of higher surface velocity are likely due to large ice fluxes being funneled through relatively narrow valleys, changes in basal conditions (transition from cold to warm bed), and increases in driving stress. Higher velocities on coastal glaciers are also likely driven by high accumulation rates due to their proximity to Baffin Bay. These patterns of ice motion are similar to those found in the northern CAA (Van Wychen et al. 2014).

The "central" region of the study site includes the small glaciers and ice caps that fringe the central coastline of Baffin Island (Figs. 3*a*, 4*b*) and Barnes Ice Cap (Fig. 3*b*). The central coastal glaciers have velocity patterns similar to those described for the "northern" coastal glaciers and the mechanisms driving flow are likely the same, although peak velocities are generally lower (~50–80 m a^{-1}). Most of the margin of Barnes Ice Cap flows at speeds of <20 m a^{-1} and terminates in a broad lobe. Surface velocities >20 m a^{-1} are only found in small areas in the north-central and south-central parts of the ice cap, with maximum motion (~80 m a^{-1}) occurring in the north-central region at the front of a large lake-terminating glacier. This region of fast flow occurs across a ~5 km wide terminus, but only propagates into the ice cap interior by ~6 km (Fig. 5*e*). In the south-central region, ice moves more slowly at a maximum rate of ~50 m a^{-1}, although the area of enhanced motion propagates further (~30 km) into the ice cap interior (Fig. 5*f*). This area of faster ice flow coincides with a

Fig. 5. Solid lines denote centreline glacier velocities for select glaciers on (*a*–*d*) Bylot Island Ice Cap, (*e*–*f*) Barnes Ice Cap, and (*g*–*j*) Penny Ice Cap. Exact locations of each centreline are presented in Figs. 2–4. Dashed lines indicate the surface elevation profile of each glacier as extracted from the 1:250 000 Canadian Digital Elevation Dataset (CDED).

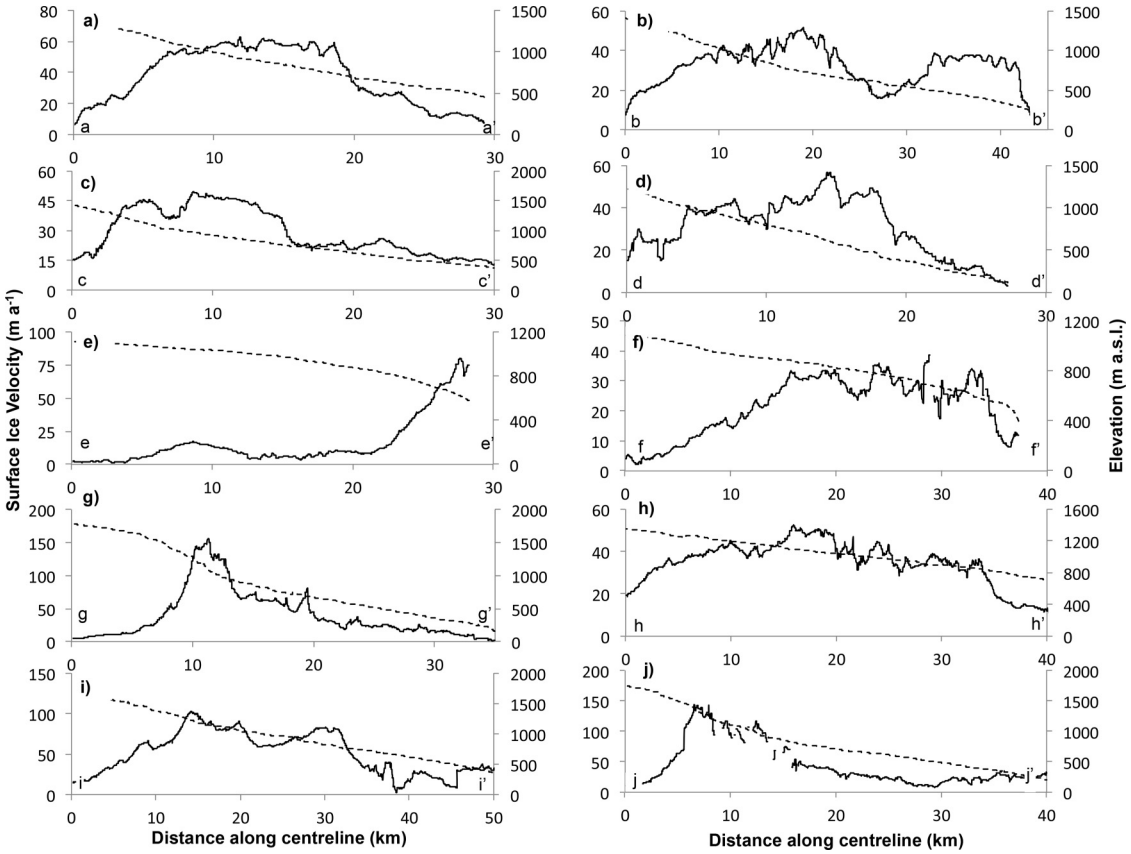

glacier previously identified as surge type (Løken 1969; Holdsworth 1973, 1977). Løken (1969) proposed that this region likely surged in the past due to a surface morphology that suggested surface lowering at upper elevations and surface bulges at lower elevations, and an advanced ice front position in comparison to adjacent regions. Holdsworth (1977) identified three additional regions where surge activity was likely to have occurred on Barnes Ice Cap (identified in Fig. 3*b*); our velocity results indicate that these glaciers are stagnant, suggesting that they are currently in quiescence if they are surge type.

The highest observed motion for the southern CAA is found in the "southern" region of Baffin Island and occurs on Penny Ice Cap (Fig. 4*a*), where surface velocities of ~100–120 m a^{-1} are found on the main tributary of Coronation Glacier on the east side of the ice cap and on several unnamed outlet glaciers located in the southwest, north-central, and northeastern portions of the ice cap. Slower motion of ~50–80 m a^{-1} occurs on several additional unnamed glaciers located in the western, northern, and southern regions of the ice cap (Figs. 5*g*–5*j*). Similar to the smaller coastal glaciers, higher glacier velocities on Penny Ice Cap tend to occur in areas where large areas of accumulation connect with narrow outlets, and likely reflect local changes in basal conditions and driving stress. Unlike the glaciers in the northern CAA where higher velocities are maintained from the point of initiation to the terminus, the outlet glaciers on Penny Ice Cap tend to slow from these connection points to their calving margin. Unlike the glaciers of Barnes and Bylot Island ice caps, none of the glaciers on Penny Ice Cap have previously been identified as surge type, and a visual analysis of historical Landsat imagery shows no evidence that would classify them as such (e.g., looped–distorted moraines, potholes, extensive crevassing, dramatic terminus advance–retreat).

The surface velocities of the southeastern coastal glaciers (Fig. 4*c*) are low, with only a few areas of motion above detection limits (30–60 m a^{-1}).

Dynamic discharge

Our calculations indicate that total mass loss via dynamic discharge from the ice masses of the southern CAA lies between ~17 Mt a^{-1} and ~108 Mt a^{-1}, with a mid-point estimate of ~55 Mt a^{-1} (Table 3). The largest contributors to dynamic discharge are located on Penny Ice Cap with Coronation Glacier (ID 44) and Unnamed Glacier (ID 43) accounting for ~19% (Q_{mid}) and ~17% (Q_{mid}) of total dynamic discharge from the southern CAA. The next largest source of dynamic discharge is an unnamed coastal glacier located on northern Baffin Island (ID 20, responsible for ~13% of total southern CAA dynamic discharge) followed by the two tidewater-terminating glaciers of Bylot Island Ice Cap (IDs 45 and 46). The total mass loss via dynamic discharge from all the glaciers on Baffin Island and Bylot Island is only ~2% of that determined for the northern CAA, with each of the eight largest glaciers (e.g., Trinity, Wykeham, Belcher, Ekblaw, Otto, Good Friday Bay, Cadogan, and Fitzroy) in the Canadian high Arctic transferring more mass to the oceans than all glaciers in the southern CAA combined (Van Wychen et al. 2014). This highlights the fact that iceberg discharge from the Canadian Arctic as a whole is dominated by a few glaciers in the northern CAA.

Gardner et al. (2011) provide the only previous estimate of dynamic discharge from Baffin Island and Bylot Island at ~250 Mt a^{-1}. Our estimate is considerably less than this, with Q_{min} ~94% less, Q_{mid} ~78% less, and Q_{max} ~57% less. This discrepancy is likely because Gardner et al. (2011) overestimated ice flux for Baffin Island and

Table 3. Estimated frontal ablation from the tidewater-terminating glaciers of Baffin Island and Bylot Island.

			Discharge (Mt a^{-1})		
Glacier ID	Lat. (°N)	Long. (°W)	$Q_{min.}$	$Q_{mid.}$	$Q_{max.}$
1	70.23	–70.63	0.3	0.9	1.7
2	70.25	–70.62	0.0	0.2	1.0
3	70.33	–70.60	0.0	0.1	0.7
4	66.60	–62.07	0.6	1.5	2.6
5	69.73	–69.81	0.0	0.2	0.5
6	69.92	–70.14	0.0	0.4	1.2
7	70.52	–71.68	0.0	0.5	1.2
8	70.45	–71.85	0.0	0.8	2.2
9	70.42	–71.98	0.5	1.2	2.0
10	70.54	–71.20	0.1	0.5	1.0
11	70.92	–72.33	0.0	0.2	0.7
12	71.05	–73.33	0.0	0.1	0.2
13	71.07	–73.26	0.0	0.1	0.4
14	71.11	–73.21	0.1	0.3	0.7
15	71.17	–73.16	0.0	0.1	0.4
16	72.01	–75.21	0.3	1.0	1.7
17	72.11	–74.87	0.0	0.2	0.8
18	71.74	–74.83	0.0	0.4	1.0
19	71.79	–75.69	0.0	0.1	0.3
20	71.87	–75.69	3.5	7.2	10.4
21	72.05	–75.99	0.0	0.1	0.2
22	72.09	–75.83	0.0	0.1	0.2
23	71.94	–75.62	1.7	3.7	5.6
24	71.73	–75.84	0.7	1.5	2.2
25	71.89	–76.25	0.1	0.3	0.7
26	72.00	–76.03	0.2	0.7	1.4
27	72.07	–75.92	0.1	0.3	0.6
28	72.61	–76.43	0.0	0.1	0.3
29	72.46	–76.07	0.0	0.2	0.6
30	72.14	–75.70	0.0	0.3	1.9
31	72.11	–75.90	0.0	0.2	0.4
32	72.07	–76.04	0.0	0.1	0.4
33	71.92	–76.31	0.2	0.6	1.2
34	71.85	–76.40	0.0	0.1	0.5
35	73.24	–81.13	0.0	0.2	0.5
36	73.23	–81.06	0.3	0.8	1.4
37	69.32	–69.17	0.0	0.5	1.3
38	69.58	–68.65	0.0	0.4	1.0
39	71.36	–73.96	0.0	0.3	0.6
40	71.44	–73.87	0.0	0.1	0.4
41	71.59	–74.53	0.1	0.4	0.8
42	71.59	–74.25	0.0	0.2	0.6
43	67.58	–66.02	3.3	10.6	19.3
44	67.19	–64.83	2.7	9.3	17.5
45	73.68	–80.10	0.5	2.2	5.0
46	73.64	–79.55	1.2	5.6	12.6
Total discharge			16.6	54.7	107.9

Note: Bold glacier ID numbers denote glaciers where the "outlet glacier" scenario was used to estimate ice thickness, all other glaciers used the "valley glacier" scenario to estimate ice thickness.

Bylot Island because they used previously published flux estimates from the Northern Canadian Arctic (e.g., Williamson et al. 2008; Burgess et al. 2005) to determine an average mass discharge per unit of terminus width and applied this value to the widths of all tidewater terminating glaciers on Baffin Island and Bylot Island. There are two problems with this approach. First, the outlet glaciers in the Northern Canadian Arctic are generally faster flowing (typically ~150–250 m a^{-1} at their calving fronts (Van Wychen et al. 2014)) than those in the Southern Canadian Arctic (typically 20–60 m a^{-1} at their calving front), which would lead to an erroneously high discharge rate per terminus width when applied to the southern Canadian Arctic. Second, Gardner et al. (2011), in part, based their average terminus width discharge rate on the flux rates provided by (Williamson et al. 2008), who used a box shape to represent glacier geometry, rather than the more realistic U shape that we utilize here. Williamson et al. (2008) also derived glacier velocities using feature tracking of optical imagery, which provides velocity results in areas with distinct surface features (e.g., crevasses) that are located in faster flow regions of the terminus. This means that the surface velocities used by Williamson et al. (2008) to calculate ice flux were likely biased to faster flowing regions, which would also lead to higher average rates of mass flux per terminus width. To assess these effects, we extract the glacier centerline velocity (i.e., areas of fast flow) of all glaciers in our study region and combine it with a box-shaped glacier geometry for each ice thickness scenario, using this approach increases the ice flux by ~276% for the Q_{min} scenario, ~207% for the Q_{mid} scenario, and ~135% for the Q_{max} scenario. We, therefore, believe that our results are an improvement on previous ice flux estimates, as they use more realistic glacier geometries and surface velocities across the calving front.

To determine the relative importance of iceberg calving as a regional ablation mechanism, our estimate of dynamic discharge can be compared with estimates of ice loss via surface melt and runoff derived from surface mass balance model driven by the output of the Regional Atmospheric Climate Model (RACMO2) and corrected for evolving glacier hypsometry (Lenaerts et al. 2013). In 2011, Q_{mid} accounted for ~0.11% (0.054 Gt a^{-1}) of total ablation of 47.5 Gt a^{-1}. The average mass loss via surface melt and runoff between 2007 and 2011 was ~53.5 Gt a^{-1}, so dynamic discharge was even less important in these earlier years (J. Lenaerts, personal communication, 2015). The proportional importance of dynamic discharge compared to surface melt and runoff for Baffin Island and Bylot Island is considerably smaller than in the northern CAA, where iceberg discharge accounted for ~3.1% of total ablation in 2012 (Van Wychen et al. 2014).

Conclusions

The surface velocity structure of the ice masses of Baffin Island and Bylot Island is broadly similar to that of the ice masses located in the northern CAA, with slow-moving (<20 m a^{-1}) interior regions contrasting with areas of faster motion where tributaries and outlet glaciers discharge from the ice cap interior. The regions of speed-up likely arise due to ice from large accumulation areas being forced through relatively narrow valleys at lower altitudes, changes in basal conditions from a cold to a warm bed, and increases in driving stress as surface slopes steepen and ice thicknesses reach a maximum. However, in contrast to the northern CAA, where higher ice motion is typically maintained from the point of speed-up in the upper ablation area to the glacier snout, glaciers of the southern CAA typically attain maximum velocities along their mid to upper ablation areas, and decelerate towards their termini.

Calculations based on the surface velocity and estimated ice thickness at the terminus of the 46 tidewater glaciers on Baffin Island and Bylot Island indicates a regional dynamic discharge rate between ~17 Mt a^{-1} and ~108 Mt a^{-1}, with a mid-scenario estimate of ~55 Mt a^{-1}. This estimate of iceberg discharge is less than previously derived for the region by Gardner et al. (2011) and is only ~2% of that for the northern CAA. Van Wychen et al. (2014) provided a comparison of iceberg discharge volumes for all reported Arctic glaciated regions (including the ice masses of Baffin Island and Bylot Island based on the discharge estimate of Gardner et al. (2011)) and showed that the southern CAA was responsible for 0.7% of total Arctic dynamic discharge. Using our revised Q_{mid} estimate of discharge, this number can be revised downwards, such that the ice masses of Baffin Island and Bylot Island are currently responsible for ~0.14% of total Arctic dynamic discharge. Comparison with outputs from regional climate models indicate that dynamic discharge in the southern CAA only accounts for a small proportion of total ice loss there (~0.11% in 2011 based on the Q_{mid} estimate of discharge), which further high-

lights the fact that currently observed mass loss in the Canadian Arctic is dominated by surface melt and runoff, rather than dynamic discharge (iceberg calving).

Future acquisitions of ice thickness datasets, updated regional digital elevation models, and investigations of basal conditions in regions of faster ice motion would all be beneficial to advance the knowledge of the controls on glacier dynamics within the southern CAA. Continued velocity mapping will enable the temporal evolution of surface velocities to be determined and aid with the identification of surge-type glaciers and help refine the length and peak velocities of surges.

Acknowledgements

We thank NSERC, Canada Foundation for Innovation, Ontario Research Fund, ArcticNet, Ontario Graduate Scholarship, University of Ottawa, Polar Continental Shelf Program, and the NSERC Canada Graduate Scholarship for funding. Support for D.O.B. was provided through the Climate Change Geoscience Program, Earth Sciences Sector (contribution No. 20150077), Natural Resources Canada. ALOS PALSAR data were obtained through the Alaska Satellite Facility. Parks Canada, Christian Zdanowicz, and various field assistants are gratefully acknowledged for assistance with fieldwork on Penny Ice Cap.

References

Burgess, D.O., Sharp, M.J., Mair, D.W.F., Dowdeswell, J.A., and Benham, T.J. 2005. Flow dynamics and iceberg calving rates of Devon Ice Cap, Nunavut, Canada. Journal of Glaciology, **51**(173): 219–230. doi:10.3189/172756505781829430.

Burgess, E.W., Foster, R.R., and Larsen, C.F. 2013. Flow velocities of Alaskan glaciers. Nature Communications, **4**: 1–8. doi:10.1038/ncomms3146.

Dowdeswell, E.K., Dowdeswell, J.A., and Cawkwell, F. 2007. On the glaciers of Bylot Island, Nunavut, Arctic Canada. Arctic, Antarctic, and Alpine Research, **39**(3): 402–4011. doi:10.1657/1523-0430(05-123)[DOWDESWELL]2.0.CO;2.

Dupont, F., Royer, A., Langlois, A., Gressent, A., Picard, G., Fily, M., et al. 2012. Monitoring the melt season length of the Barnes Ice Cap over the 1979–2010 period using active and passive microwave remote sensing data. Hydrological Processes, **26**: 2643–2652. doi:10.1002/hyp.9382.

Gardner, A.S., Moholdt, G., Wouters, B., Wolken, G.J., Burgess, D.O., Sharp, M.J., et al. 2011. Sharply increased mass loss from glaciers and ice caps in the Canadian Arctic Archipelago. Nature, **473**(7347): 357–360. doi:10.1038/nature10089. PMID:21508960.

Gardner, A., Moholdt, G., Arendt, A., and Wouters, B. 2012. Accelerated contributions of Canada's Baffin and Bylot Island glaciers to sea level rise over the past half century. The Cryosphere, **6**: 1103–1125. doi:10.5194/tc-6-1103-2012.

Gogineni, P. 2012. Radar Depth Sounder Data Products. Lawrence, Kansas, USA. Digital media. http://data.cresis.ku.edu/.

Gray, A.L., Mattar, K.E., and Sofko, G. 2000. Influence of ionospheric electron density fluctuations on satellite radar interferometry. Geophysical Research Letters, **27**(10): 1451–1454. doi:10.1029/2000GL000016.

Gray, A.L., Short, N., Mattar, K.E., and Jezek, K.C. 2001. Velocities and flux of the Filchner Ice Shelf and its tributaries determined from speckle tracking interferometry. Canadian Journal of Remote Sensing, **27**(3): 193–206. doi:10.1080/07038992.2001.10854936.

Harbor, J.M. 1992. Numerical modeling of the development of U-shaped valleys by glacier erosion. Geological Survey of America Bulletin, **104**(10): 1364–1375. doi:10.1130/0016-7606(1992)104<1364:NMOTDO>2.3.CO;2.

Heid, T., and Kääb, A. 2012. Repeat optical satellite images reveal widespread and long term decrease in land-terminating glacier speeds. The Cryosphere, **6**: 467–478. doi:10.5194/tc-6-467-2012.

Holdsworth, G. 1973. Evidence of a surge on Barnes Ice Cap, Baffin Island. Canadian Journal of Earth Sciences, **10**: 1565–1574. doi:10.1139/e73-148.

Holdsworth, G. 1977. Surge activity on the Barnes Ice Cap. Nature, **269**: 588–590. doi:10.1038/269588a0.

Lenaerts, J.T.M., van Angelen, J.H., van den Broeke, M.R., Gardner, A.S., Wouters, B., and van Meijgaard, E. 2013. Irreversible mass loss of Canadian Arctic Archipelago glaciers. Geophysical Research Letters, **40**: 870–874. doi:10.1002/grl.50214.

Løken, O.H. 1969. Evidence of surges on the Barnes Ice Cap, Baffin Island. Canadian Journal of Earth Sciences, **6**: 899–901. doi:10.1139/e69-093.

Paterson, W.S.B. 1994. The physics of glaciers, 3rd edition. Elsevier, Oxford.

Rosen, P.A., Jet Propulsion, Lab, Hensley, S., Joughin, I.R., Li, F.K., Madsen, S.N., et al. 2000. Synthetic aperture radar interferometry. Proceedings of the IEEE, **88**(3): 333–382. doi:10.1109/5.838084.

Sharp, M., Burgess, D.O., Cawkwell, F., Copland, L., Davis, J.A., Dowdeswell, E.K., et al. 2014. Remote sensing of recent glacier changes in the Canadian Arctic. *In* Global Land Ice Measurements from Space. *Edited by* J.S. Kargel, G.J. Leonard, M.P. Bishop, A. Kääb, and B.H. Raup. Praxis-Springer. Ch. 9, pp. 205–228. doi:10.1007/978-3-540-79818-7_9.

Short, N.H., and Gray, A.L. 2005. Glacier dynamics in the Canadian High Arctic from RADARSAT-1 speckle tracking. Canadian Journal of Remote Sensing, **31**(3): 225–239. doi:10.5589/m05-010.

Strozzi, T., Luckman, A., Murray, T., Wegmuller, U., and Werner, C.L. 2002. Glacier motion estimation using SAR offset-tracking procedures. IEEE Transactions on Geoscience and Remote Sensing, **40**(11): 2384–2391. doi:10.1109/TGRS.2002.805079.

Van Wychen, W., Copland, L., Gray, L., Burgess, D.O., Danielson, B., and Sharp, M. . 2012. Spatial and temporal variation of ice motion and ice flux from Devon Ice Cap, Nunavut, Canada. Journal of Glaciology, **58**(210): 657–664. doi:10.3189/2012JoG11J164.

Van Wychen, W., Burgess, D.O., Gray, L., Copland, L., Sharp, M., Dowdeswell, J.A., and Benham, T.J. 2014. Glacier velocities and dynamic ice discharge from the Queen Elizabeth Islands, Nunavut, Canada. Geophysical Research Letters, **41**: 484–490. doi:10.1002/2013GL058558.

Waechter, A., Copland, L., and Herdes, E. 2015. Modern glacier velocities across the Icefield Ranges, St. Elias Mountains, and variability at selected glaciers from 1959 to 2012. Journal of Glaciology. **61**(228): 624–634. doi:10.3189/2015JoG14J147.

Wainstein, P., Moorman, B., and Whitehead, K. 2014. Glacial conditions that contribute to the regeneration of Fountain Glacier proglacier icing, Bylot Island, Canada. Hydrological Processes, **28**: 2749–2760. doi:10.1002/hyp.9787.

Williamson, S., Sharp, M., Dowdeswell, J., and Benham, T. 2008. Iceberg calving rates from northern Ellesmere Island ice caps, Canadian Arctic, 1999–2003. Journal of Glaciology, **54**(186): 391–400. doi:10.3189/002214308785837048.

Zdanowicz, C., Smetny-Sowa, A., Fisher, D., Schaffer, N., Copland, L., Eley, J., and Dupont, F. 2012. Summer melt rates on Penny Ice Cap, Baffin Island: past and recent trends and implications for regional climate. Journal of Geophysical Research, **117**: F02006. doi:10.1029/2011JF002248.